

Supporting Information for

Ferrovalleytricity in Two-Dimensional Antiferromagnetic Lattice

Shuyan Chai,¹ Yangyang Feng,¹ Ying Dai,^{*,1} BaibiaoHuang,¹ Liangzhi Kou,^{*,2} Yandong Ma^{*,1}

¹School of Physics, State Key Laboratory of Crystal Materials, Shandong University, Jinan 250100, China;

²School of Mechanical, Medical and Process Engineering, Queensland University of Technology, Brisbane,

Queensland 4001, Australia;

*Corresponding author: daiy60@sina.com (Y.D.); liangzhi.kou@qut.edu.au (L.K.);
yandong.ma@sdu.edu.cn (Y.M.)

Note 1. Methods

First-principles calculations are performed based on density functional theory (DFT) [1] within the generalized gradient approximation of the Perdew-Burke-Ernzerhof (PBE) functional [2], and implemented in the Vienna ab initio simulation package (VASP) [3]. The plane-wave basis set with a kinetic energy cutoff of 500 eV is considered. The system is relaxed until the energy is converged to 10^{-6} eV and the forces are less than 0.001 eV/Å. The Monkhorst-Pack k-point meshes used are $7 \times 7 \times 1$ for sampling the Brillouin zone. To describe the strong correlation effect for the localized 3d electrons of Mn and Cr atoms, the effective on-site Hubbard terms of $U = 5$ eV and $U = 3$ eV are utilized, respectively [4]. The spin-orbit coupling (SOC) is included in the calculations. To avoid spurious interactions between periodic images, a vacuum space of at least 20 Å is introduced. Grimme's DFT-D3 method is employed to describe the van der Waals interactions [5]. The dipole moment correction is employed to evaluate the vertical electric polarization [6]. Berry curvature is calculated with employing VASPBERRY [7].

Note 2. $k \cdot p$ model

As shown in **Figure 1(a)**, \mathbf{R}_i ($i = 1-6$) and \mathbf{r}_j ($j = 1-3$) represent the six next nearest neighbor and the three nearest neighbor lattice vectors, respectively. Based on this lattice structure, the next nearest neighbor transitions are represented by \mathbf{R}_i ($i = 1-6$) to determine the diagonal components and the nearest neighbor transitions are represented by \mathbf{r}_j ($j = 1-3$) to determine the off-diagonal components [8]. Under the D_{6h} symmetry, the d orbitals of Mn atom split into A_{1g} (d_{z^2}), E_{1g} (d_{xz} , d_{yz}) and E_{2g} ($d_{x^2-y^2}$, d_{xy}). The basis d_{xz} and d_{yz} of irreducible representation E_{1g} are selected as the basis functions. And it is consistent with the main contribution orbitals of the Mn atom at VBM and CBM in MnPSe₃ [as shown in **Figure S1(a)** and **S1(b)**]. The next nearest neighbor transitions and nearest neighbor transitions Hamiltonians near K and K' valleys are given as:

$$H_0^{A(B)}(k) = \begin{bmatrix} \varepsilon + t(q_x^2 + q_y^2) & 0 \\ 0 & \varepsilon + t(q_x^2 + q_y^2) \end{bmatrix}$$

and

$$H^{AB}(k) = \begin{bmatrix} d(q_x + iq_y) + g(\tau q_x + iq_y)^2 & 0 \\ 0 & -d(q_x + iq_y) - g(\tau q_x + iq_y)^2 \end{bmatrix}$$

where ε is a correction energy bound up with the Fermi energy, $q = k - K$ is the momentum vector and t, d, g are parameters related to hopping strength. So, the total Hamiltonian with external ZMF around the K and K' points is given by the following:

$$H(k) = \begin{bmatrix} m + \varepsilon + t(q_x^2 + q_y^2) + \tau\lambda_c + bm_c & 0 & d(q_x - iq_y) + g(\tau q_x - iq_y)^2 & 0 \\ 0 & -m + \varepsilon + t(q_x^2 + q_y^2) - \tau\lambda_v - bm_v & 0 & -d(q_x - iq_y) - g(\tau q_x - iq_y)^2 \\ d(q_x + iq_y) + g(\tau q_x + iq_y)^2 & 0 & -m + \varepsilon + t(q_x^2 + q_y^2) - \tau\lambda_c + bm_c & 0 \\ 0 & -d(q_x + iq_y) - g(\tau q_x + iq_y)^2 & 0 & m + \varepsilon + t(q_x^2 + q_y^2) + \tau\lambda_v - bm_v \end{bmatrix}$$

It is consistent with the description of heterotrilinear CrBr₃-MnPSe₃-CrBr₃ by VASP [**Figure S1(c)** and **(d)**].

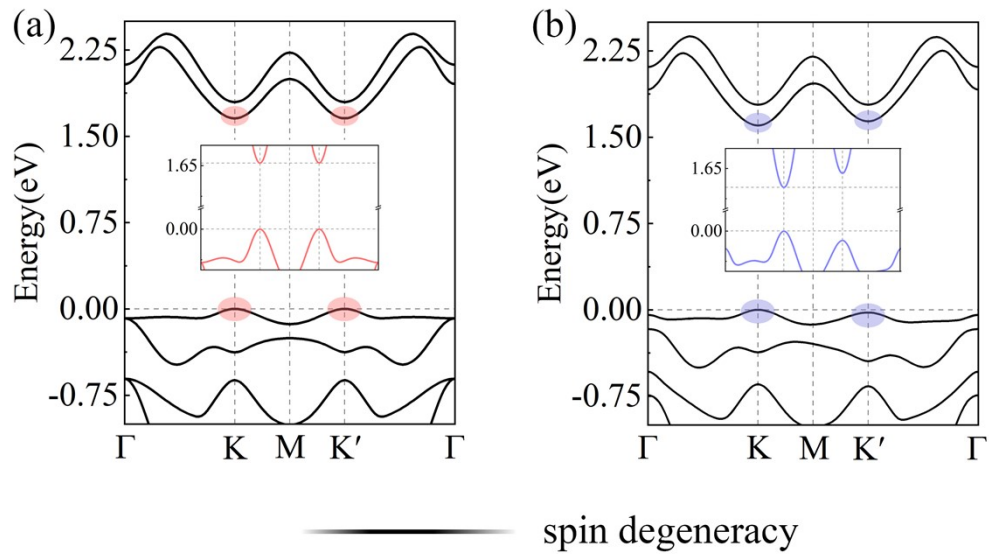


Figure S1. Spin-polarized band structures of monolayer MnPSe₃ (a) without and (b) with SOC.

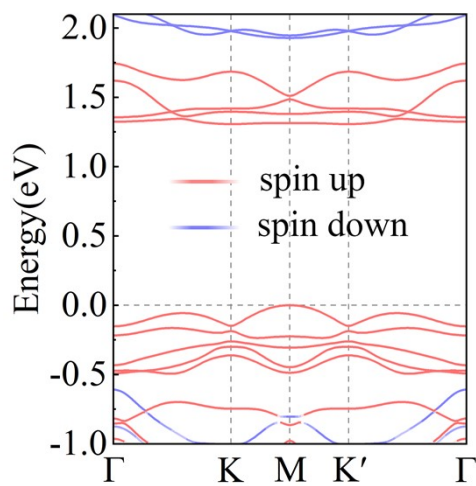


Figure S2. Spin-polarized band structure of monolayer CrBr₃ with SOC.

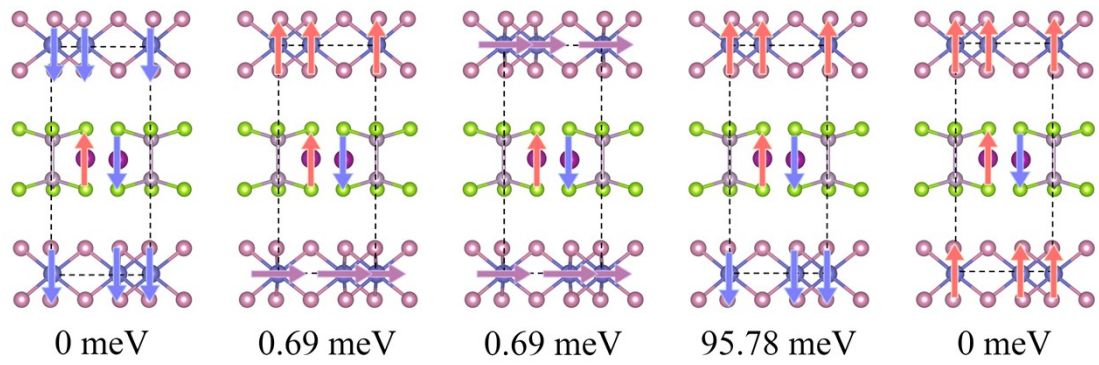


Figure S3. Magnetic configurations of heterotrilayer $\text{CrBr}_3\text{-MnPSe}_3\text{-CrBr}_3$. The values represent the energies with reference to the lowest energy state.

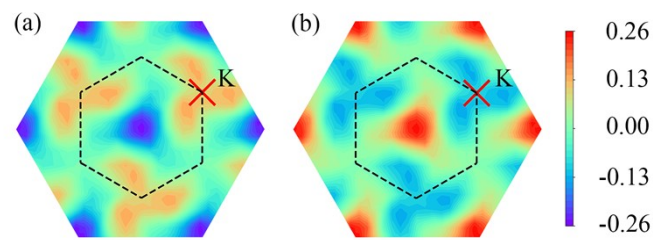


Figure S4. Berry curvatures of heterotrilayer $\text{CrBr}_3\text{-MnPSe}_3\text{-CrBr}_3$ in (a) state-1 and (b) state-2 as a counter map over the 2D Brillouin zone.

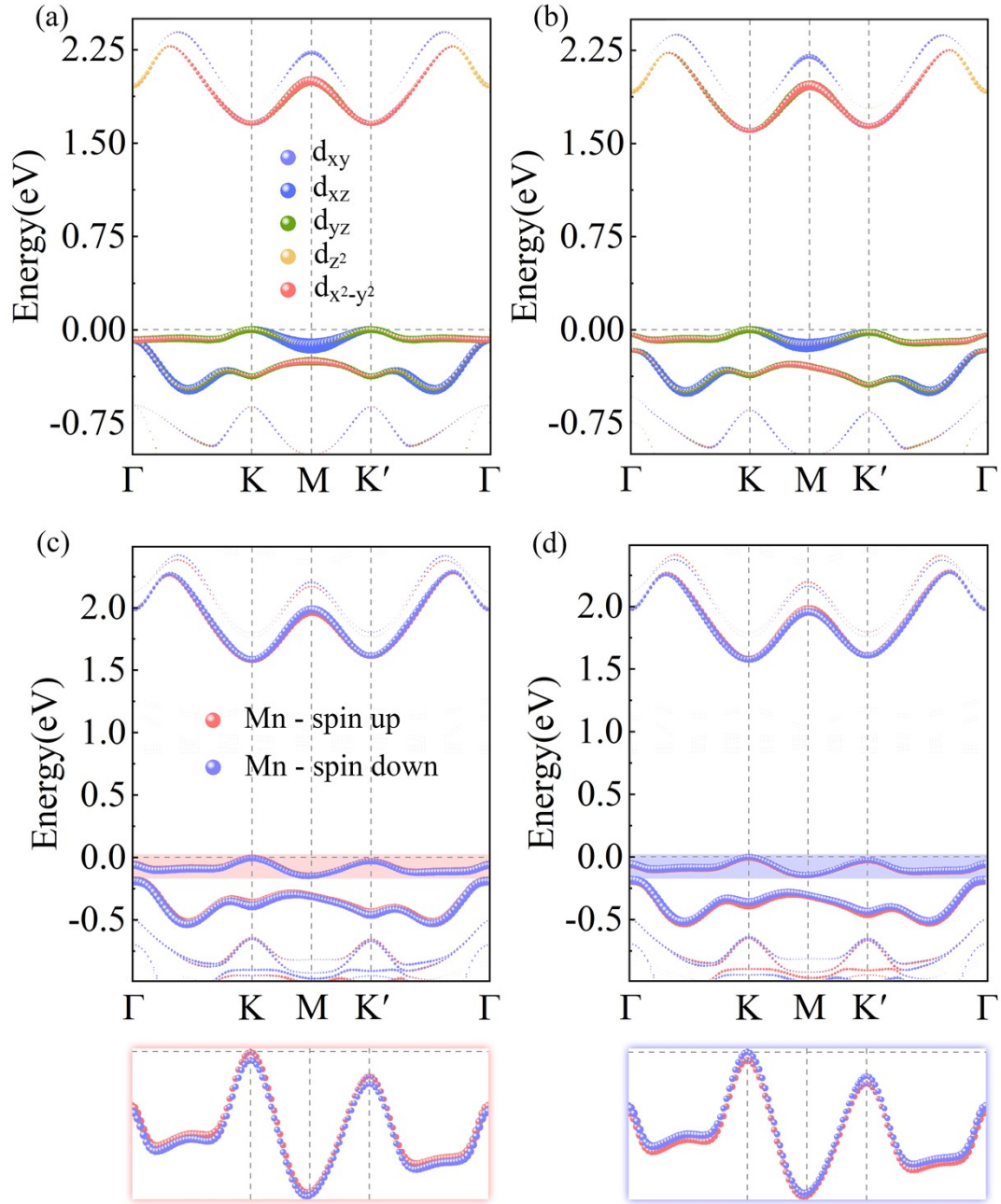


Figure S5. Orbital-resolved band structures of monolayer MnPSe₃ (a) with and (b) without SOC. Atom-resolved band structures of heterotrilayer CrBr₃-MnPSe₃-CrBr₃ in (c) state-1 and (d) state-2 with SOC. The bottom panels are the enlarged one corresponding to the shaded parts in the top panels.

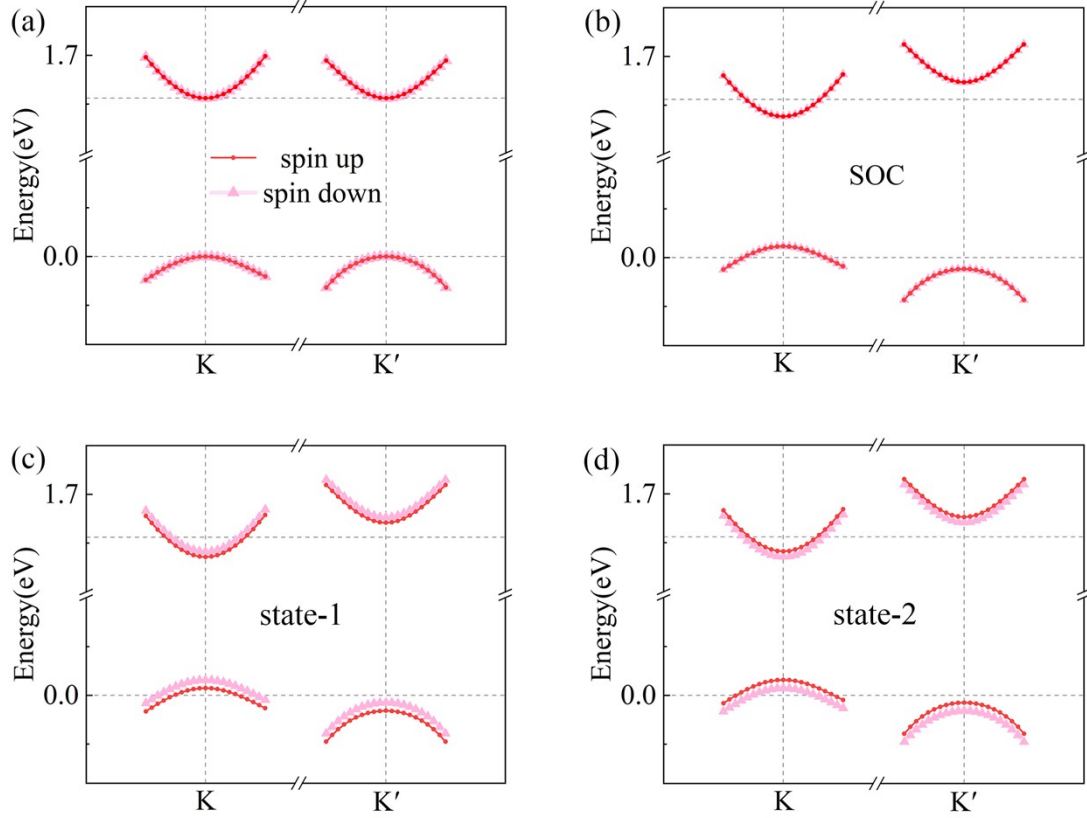


Figure S6. Low-energy conduction and valence band dispersions around the K and K' valleys for (a) monolayer MnPSe₃ without SOC, (b) monolayer MnPSe₃ with SOC, heterotrilayer CrBr₃-MnPSe₃-CrBr₃ in (c) state-1 and (d) state-2 with SOC obtained from the $k\cdot p$ model.

References

1. W. Kohn and L. Sham, Self-consistent equations including exchange and correlation effects, Phys. Rev.140, A1133 (1965).
2. J. P. Perdew, K. Burke, and M. Ernzerhof, Generalized gradient approximation made simple. Phys. Rev. Lett. 78, 1396–1396 (1997).
3. G. Kresse and J. Furthmüller, Efficiency of ab-initio total energy calculations for metals and semiconductors using a plane-wave basis set. Comput. Mater. Sci. 6, 15–50 (1996).
4. H. Li and W. Zhu, Spin-driven ferroelectricity in two-dimensional magnetic heterostructures, Nano Lett. 23, 22, 10651–10656 (2023).

5. S. Grimme, J. Antony, S. Ehrlich and S. Krieg, A consistent and accurate ab initio parametrization of density functional dispersion correction (DFT-D) for the 94 elements H-Pu, *J. Chem. Phys.* 132, 154104 (2010).
6. R. King-Smith and D. Vanderbilt, Theory of polarization of crystalline solids, *Phys. Rev. B* 47, 1651 (1993).
7. T. Fukui, Y. Hatsugai and H. Suzuki, Chern numbers in discretized Brillouin zone: Efficient method of computing (spin) Hall conductances, *J. Phys. Soc. Jap.*, 2005, 74, 1674.
8. K. Das, K. Ghorai, D. Culcer and amit agarwal, nonlinear valley Hall effect, *Phys. Rev. Lett.* 132, 096302 (2024).